

Real-time Speech Enhancement on Raw Signals with Deep State-space Modeling

Yan Ru Pei¹, Ritik Shrivastava¹, FNU Sidharth¹

¹Research, BrainChip, USA

yanrpei@gmail.com, rshrivastava@brainchip.com, sidharth@brainchip.com

Abstract

We present aTENNuate, a simple deep state-space autoencoder configured for efficient online raw speech enhancement in an end-to-end fashion. The network’s performance is primarily evaluated on raw speech denoising, with additional assessments on tasks such as super-resolution and de-quantization. We benchmark aTENNuate on the VoiceBank + DEMAND and the Microsoft DNS1 synthetic test sets. The network outperforms previous real-time denoising models in terms of PESQ score, parameter count, MACs, and latency. Even as a raw waveform processing model, the model maintains high fidelity to the clean signal with minimal audible artifacts. In addition, the model remains performant even when the noisy input is compressed down to 4000Hz and 4 bits, suggesting general speech enhancement capabilities in low-resource environments. Source code is available at github.com/Brainchip-Inc/aTENNuate/

Index Terms: state-space models, autoencoder, denoising, super-resolution, de-quantization

1. Introduction

Speech enhancement is crucial for improving both human-to-human communication, such as in hearing aids, and human-to-machine communication, as seen in automatic speech recognition (ASR) systems. A challenging task of speech enhancement is removing background noises from speech signals, where the complexity of speech and noise patterns poses challenges. [1]. Traditional speech enhancement methods such as Wiener filtering [2], spectral subtraction [3], and principal component analysis [4] have shown satisfactory performance in stationary noise environments, but their effectiveness is often limited in non-stationary noise scenarios, resulting in artifacts such as musical noises and substantial degradation in both the quality and intelligibility of the enhanced speech [5].

Deep learning audio denoising methods are trained on large datasets of clean and noisy audio pairs, and attempt to capture the nonlinear relationship between the noisy and clean signal features without prior knowledge of the noise statistics, as required by traditional denoising methods [6]. Speech features can be extracted from real or complex spectrograms of the noisy signal in the time-frequency domain, or the raw waveform [7].

Many state-of-the-art deep learning denoising models leverage the feature extraction capability of convolutional networks. The UNet convolutional encoder-decoder is a common network architecture in denoising models [8, 9, 10] exemplified by Deep Complex UNet [11] and the generative adversarial SEGAN [12]. However, CNNs lack the capabilities to model long-range temporal dependencies present in speech signals, without incurring significant memory resources [13]. Another class of models that are more capable in this regard are RNNs, examples of

which are DCCRN [14] and FRCRN [15]. However, these models typically show limited robustness to different types of noise and generalization across diverse audio sources [16]. Most importantly, their non-linear recurrent nature prevents efficient usage of parallel hardware (e.g. GPUs) for training, which limits their potential for scaling.

Alternative approaches such as PercepNet [17] and RN-Noise [18] have attempted to reduce network size and complexity by combining traditional speech enhancement methods with deep learning, resulting in smaller models with fewer parameters capable of running in real-time on general-purpose hardware. Similarly, methods that process raw waveform signals aim to maximize the expressive capabilities of deep networks without resorting to hand-engineered spectral conversions, as demonstrated by Facebook’s DEMUCS model’s real-time performance [19]. However, the majority of these models cannot perform real-time inference on general-purpose hardware, exemplified by Nvidia’s CleanUNet model [20]. Models such as DeepFilterNet [21] have leveraged speech-specific properties such as short-time speech correlations to achieve comparable results.

Here, we introduce the aTENNuate network, belonging to the class of Temporal Neural Networks (TENNns). It is a deep state-space model (SSM) [22, 23] optimized for real-time denoising of raw speech waveforms on the edge. By virtue of being a state-space model, the model is capable of capturing long-range temporal relationships present in speech signals, with stable linear recurrent units. Learning long-range correlations can be useful for capturing global speech patterns or noise profiles, and perhaps implicitly capture semantic contexts to aid speech enhancement performance [24].

During the training of the aTENNuate network, we can use the infinite impulse response (IIR) kernels of the SSM layers as long convolutional kernels over the input features, which can be parallelized using techniques such as FFT convolution [25] or associative scan [26]. During inference, the temporal convolution layers can be converted into equivalent recurrent layers for efficient real-time processing on mobile devices, minimizing latency and reducing the need for excessive buffering of data.

The evaluation code of a pre-trained aTENNuate network is available at our Github repo [Brainchip-Inc/aTENNuate](https://github.com/Brainchip-Inc/aTENNuate).

2. State-space Modeling

In this section, we briefly describe what state-space models are, and recall how they can be configured for neural network processing, involving discretization and diagonalization. State-space models are general representations of linear time-invariant (LTI) systems, and they can be uniquely specified by four matrices: $A \in \mathbb{R}^{h \times h}$, $B \in \mathbb{R}^{h \times n}$, $C \in \mathbb{R}^{m \times h}$, and

$D \in \mathbb{R}^{m \times n}$. The first-order ODE describing the LTI system is given as

$$\dot{x} = Ax + Bu, \quad y = Cx + Du, \quad (1)$$

where $u \in \mathbb{R}^n$ is the input signal, $x \in \mathbb{R}^h$ is the internal state, and $y \in \mathbb{R}^m$ is the output. Here, we are letting $n > 1$, $m > 1$, which yields a multiple-input, multiple-output (MIMO) state-space model. For the remainder of this paper, we will ignore the Du term as it effectively serves as a skip connection [25], which is already included explicitly in our network (see Fig. 1).

The state-space model in its original form describes a continuous-time system, but in the field of digital signal processing, there are standard recipes for discretizing such a system into a discrete-time state-space model. One such method that we use in this work is the zero-order hold (ZOH), which gives us the discrete-time state-space matrices \bar{A} and \bar{B} as follows:

$$\bar{A} = \exp(\Delta A), \quad \bar{B} = (\Delta A)^{-1} \cdot (\exp(\Delta A) - 1) \cdot \Delta B. \quad (2)$$

The discrete state-space model is then given by

$$x[t+1] = \bar{A}x[t] + \bar{B}u[t], \quad y[t] = Cx[t] \quad (3)$$

In the context of recurrent neural networks (RNNs), this is essentially a linear RNN layer, which allows for efficient online inference and generation (in our case real-time speech enhancement), but at the same time efficient parallelization during training.

It is straightforward to check that the discrete-time impulse response is given as

$$k[\tau] = C \bar{A}^{\tau} \bar{B}, \quad (4)$$

where τ denotes the kernel timestep. During training, k can be considered the “full” long 1D convolutional kernel with shape (output channels, input channels, length), in the sense that the output y can be computed via the long convolution $y_j = \sum_i u_i * k_{ij}$. By the convolution theorem, we can perform this operation in the frequency domain, which becomes a point-wise product $\hat{y}_{jf} = \sum_i \hat{u}_i \hat{k}_{ijf}$. The hat symbol denotes the Fourier transform of the signal (with the index f denoting the Fourier modes), which can be efficiently computed via Fast Fourier Transforms (FFTs).

It is a generic property (though not always true) that a diagonal form exists for the state-space model, meaning that we can almost always assume \bar{A} to be diagonal [25], at the expense of potentially requiring \bar{B} and C to be complex matrices. Since the original system is a real system, the diagonal \bar{A} matrix can only contain real elements and/or complex elements in conjugate pairs. (See Appendix A for an elementary demonstration of this fact using the impulse response.) In this work, we sacrifice a slight loss in expressivity by continuing to restrict \bar{B} and C to be real matrices and letting A be a diagonal matrix with all complex elements (but not restricting them to come in conjugate pairs). Since we still want to work with real features¹, we then only take the real part of the impulse response kernel as such:

$$k[\tau] = \Re(C \bar{A}^{\tau} \bar{B}), \quad (5)$$

which equivalently in the state-space equation can be achieved by simply letting $y[t] = C \Re(x[t])$. This means that during

¹This is *a priori* not required, as technically we can configure our network as complex-valued to handle complex features. However, we do not explore this configuration in this work.

online inference, we need to maintain the internal states x as complex values, but only need to propagate their real parts to the next layer.

2.1. Optimal Contractions

Similar to previous works in deep state-space modeling, we allow the parameters $\{A, B, C, \Delta\}$ to be directly learnable, which indirectly trains the kernel k . Unlike previous works in deep state-space modeling, we do not try to keep the sizes n, h, m homogeneous, to allow for more flexibility in feature extraction at each layer, mirroring the flexibility in selecting channel and kernel sizes in convolutional neural networks². The flexibility of the tensor shapes requires us to carefully choose the optimal order of operations during training to minimize the computational load [27]. This is also briefly discussed in Appendix C.

In short, in einsum notation, our SSM operations can be written as $\hat{y}_{jff} = \hat{u}_{if} B_{in} K_{nf} C_{jn}$, a series of tensor contractions (matrix multiplications). Based on the tensor shapes involved, we can select an order of operation that is memory- and compute-optimal [28]. In addition, this allows us to freely configure the network as an hourglass network (with the SSM layers in the network having different channel and temporal dimensions), without enforcing the SISO form [23, 29, 30]. This makes our network uniquely capable of handling raw audio waveforms, while retaining strong featural interactions and light computational costs.

3. Network Architecture

We use an hourglass network with long-range skip connections, similar in form to the Sashimi network [23] for audio generation. However, unlike previous works using state-space models for audio processing [23, 29, 30, 31, 32], our network directly takes in raw audio waveforms in the -1 to +1 range and outputs raw waveforms as well, with no one-hot encoding or spectral processing (e.g. STFT or iSTFT). Furthermore, we retain causality as much as possible for the sake of real-time inference, meaning that we eschew any form of bidirectional state-space layers. See Fig. 1 for a schematic drawing.

As with typical auto-encoder networks, the audio features are down-sampled in the encoder and then up-sampled in the decoder. For the re-sampling operation, we use a simple operation that squeezes/expands the temporal dimension then projects the channel dimension [23]. More formally, for a reshaping ratio of r , a sequence of features can be down-sampled and up-sampled as:

$$\begin{aligned} \text{Down: } (C_{in}, L) &\xrightarrow{\text{reshape}} (C_{in}r, L/r) \xrightarrow{\text{project}} (C_{out}, L/r) \\ \text{Up: } (C_{in}, L) &\xrightarrow{\text{reshape}} (C_{in}/r, Lr) \xrightarrow{\text{project}} (C_{out}, Lr) \end{aligned} \quad (6)$$

The baseline network uses LayerNorm layers and SiLU activations. In addition, we include a “PreConv” layer which is a depthwise 1D convolution layer with a kernel size of 3, to enable better processing of local temporal features. The PreConv operation is omitted in the 2 SSM blocks in the neck and in any block with only one channel³. See Appendix C for details on the computation of the theoretical latency for a given set of

²The size of the internal state h , can be interpreted as the degree of parametrization of a basis temporal kernel, or some implicit (dilated) “kernel size” in the frequency domain. We explore this in a future work.

³The neck operates on fully-downsampled features, and introducing PreConv layers will incur too much latency in real-time processing. We also omit PreConv layer in single-channel blocks, because it is too lossy.

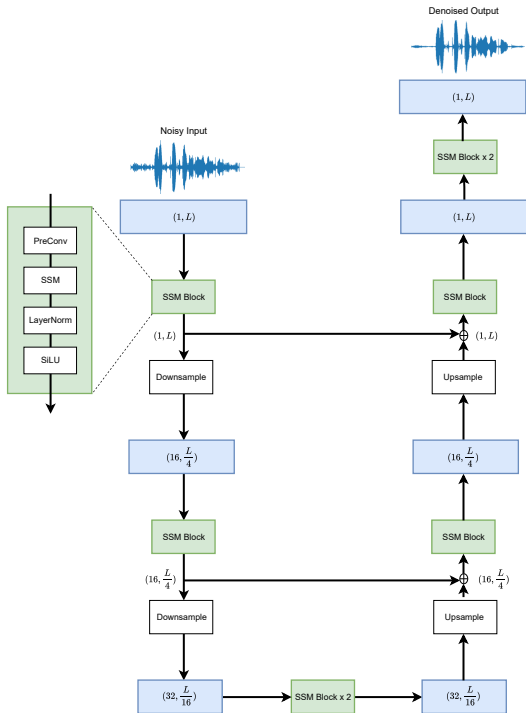


Figure 1: A schematic drawing of the network architecture, with only 2 encoder and decoder blocks shown for simplicity. The actual model has 6 encoder and decoder blocks. Note that there is no (spectral) processing on the input and output waveforms.

resampling factors and PreConv configurations. Using causal convolutions for PreConvs can eliminate additional latencies to the network [33], but we do not explore this implementation here. To better support mobile devices, we also test variants of the network with BatchNorm layers⁴, ReLU activations, and omitting PreConv layers in the decoder (and omitting PreConv layers altogether). The results are reported in the next section. The block-wise network architecture is given in Table 1, along with the PreConv latency, if present.

Table 1: Resampling factor and output channel of each block of the network, which consists of an encoder performing down-samplings, an intermediate bottleneck, a decoder performing up-samplings, and finally an output processor.

Layers	Resample Factor	Channels	Latency
Encoder			
Block 1	4	16	
Block 2	4	32	0.25ms
Block 3	2	64	1ms
Block 4	2	96	2ms
Block 5	2	128	4ms
Block 6	2	256	8ms
Neck			
Block 1	1	256	
Block 2	1	256	
Decoder			
Block 1	2	128	8ms
Block 2	2	96	4ms
Block 3	2	64	2ms
Block 4	2	32	1ms
Block 5	4	16	0.25ms
Block 6	4	1	
Output			
Block 1	1	1	
Block 2	1	1	

4. Experiments

For experiments, we train on the VCTK and LibriVox training sets downloaded from the Microsoft DNS Challenge, randomly mixed with noise samples from Audioset, Freesound, and DEMAND. We evaluate our denoising performance on the Voicebank + DEMAND (VB-DMD) testset, and the Microsoft DNS1 synthetic test set (with no reverberation) [34]. To guarantee no data leakage between the training and testing sets, we removed the clean and noise samples in the training set that were used to generate the synthetic testing samples. Both the input and output signals of the network are set at 16000 Hz. The loss function is a mix of SmoothL1Loss [35] and spectral loss at the ERB scale [21].

We train the model for 500 epochs, AdamW optimizer with a learning rate of 0.005 and a weight decay of 0.02, augmented with a cosine decay scheduler with a linear warmup of 0.01 of the total training steps. Each epoch contains the full VCTK training set, a random subset of the LibriVox training set (of

⁴Since BatchNorm is a static form of normalization during inference, the normalization statistics and the affine parameters can be “folded” into the weights and biases of the previous layer, meaning that the layer does not need to be materialized during inference.

Table 2: Comparing different variants of the aTENNuate network against other real-time audio denoising networks, in terms of performance, memory/computational requirements, and latency.

Model	PESQ (VB-DMD)	PESQ (DNS1 no-reverb)	Parameters	MACs / sec	Latency
DeepFilterNet3 [21]	3.16	2.58	2.13M	0.344G	40ms
DEMUCS [19]	2.56	2.65	33.53M ^a	7.72G ^a	40ms
PercepNet [17]	2.73 ^b	-	8.00M	0.80G	40ms
RNNNoise [18]	2.43	1.94	0.06M	0.04G	20ms
aTENNuate (base)	3.27	2.98	0.84M	0.33G	46.5ms
PreConvs only in encoder	3.21	2.84	0.84M	0.33G	31.25ms
no PreConvs	3.06	2.59	0.84M	0.33G	16ms
BatchNorm + ReLU	2.84	2.43	0.84M	0.33G	16ms

^a These numbers are estimated by passing a one-second segment of data to the model.

^b This metric is taken directly from the paper as an official implementation of the model does not exist.

ratio 0.1). To synthesize random noisy samples on the fly as inputs to the network, the clean samples are mixed randomly with the noise samples, with SNR values uniformly sampled from -5 dB to 15 dB. More details of the training pipeline are provided in Appendix B.

The evaluation metric is the average wideband PESQ score between the clean signals and the denoised outputs. The PESQ scores for different variants of the aTENNuate model against other real-time audio-denoising networks are reported in Table 2. We also report other network inference metrics including parameters, MACs, and latencies. For the latency metric, we focus on the theoretical latency of the network, not accounting for any processing latencies. In simpler terms, it is the maximum time range that the network needs to “wait” or look-forward to produce a denoised data point corresponding to the current input. As seen in Table 2, the PreConv layers (being depth-wise) does not make much difference in terms of parameters and MACs, but does add considerably to latency. Unless otherwise denoted, we use the source code and pre-trained weights of each model and run it through a standardized PESQ evaluation pipeline. In addition, we report results for other common speech-enhancement metrics in Table 3.

Table 3: Various speech enhancement metrics for the base aTENNuate network.

Testset	PESQ	CSIG	CBAK	COVL	SI-SDR
VB-DMD	3.27	4.57	2.85	3.96	15.04
DNS1	2.98	4.28	3.55	3.57	15.40

For further inspection of the quality of the denoised samples produced by the network, we listened to the denoised samples on both synthetic data and real recordings, and performed internal A/B tests against other networks. In the supplementary material, we also included the script for generating denoised audios for real recordings from the DNS1 challenge with natural reverberations. In addition, we provide a comparison of the denoised spectrogram and the clean spectrogram. This is to ensure that the denoised samples do not contain any unnatural artifacts that are common with raw audio processing systems⁵, which may not be captured by the PESQ score [36]. See Fig. 2 for the

⁵For example, the network may generate low-frequency artificial signals, resulting in a background “humming” noise. It may also attempt to aggressively attenuate high-frequency speech components, resulting in a robotic tone of speech.

spectrograms. In addition, we also try to test a homogeneous variant of the network working with spectral features (STFT + iSTFT) with a similar number of parameters and MACs, but the PESQ results were significantly worse. See Appendix D for more details

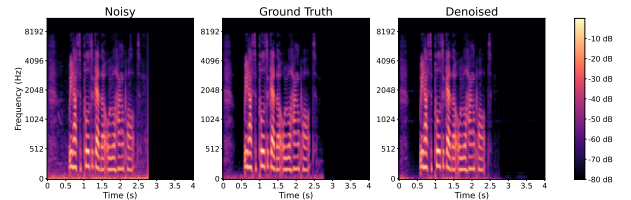


Figure 2: A comparison of the spectrograms among the noisy signal, the clean ground truth, and the denoised output of a sample in the DNS1 synthetic testset (no reverb). Besides a minor low-frequency artifact in the silent region, the denoised output matches very close to the ground truth signal, despite not using any pre/post-processing in the spectral domain.

In addition to audio denoising, we also perform studies on the ability of our network to perform super-resolution and de-quantization on highly compressed data. This involves intentionally performing down-sampling and quantization of the input signals, in that order, and re-training the network to handle the degraded/compressed inputs⁶. To use the same network architecture to interface with down-sampled audios, we perform interleaved repeats of the input signals to restore the original sample rate⁷. For quantization, we perform mu-law encoding on the input signals down to the desired bitwidth, then rescale the quantized signal back to the -1 to +1 range. The super-resolution and de-quantization results are reported in Table 4. Note that the outputs are still evaluated against clean signals at 16000 Hz and full precision.

5. Future Directions

To make the network even more mobile-friendly, we plan to explore the sparsification and quantization of the network weights and activations. Potentially, we can study a low-rank realization

⁶It is possible to perform parameter-efficient fine-tuning of a baseline model instead, such as using low-rank adaptations on the state-space matrices. We leave this to future work.

⁷An alternative is to simply remove an encoder block with the same downsampling factor as the downsampled input.

Table 4: The average PESQ scores of the model outputs when the noisy inputs are down-sampled and quantized.

Input Type	VoiceBank	DNS1
8000 Hz & 8 bit	3.19	2.88
4000 Hz & 8 bit	3.04	2.72
8000 Hz & 4 bit	2.90	2.55
4000 Hz & 4 bit	2.72	2.39

of the state-space matrices, which form the majority of the parameter count. State-space models are also known to be easily adaptable for a spiking implementation on neuromorphic hardware, so it will also be interesting to see whether our model admits an efficient spiking neural network realization, which will further reduce the power required for the solution.

6. Conclusion

We introduced a lightweight deep state-space autoencoder, aTENNuate, that can perform raw audio denoising, super-resolution, and de-quantization. Compared to previous works, the key features of this network are: 1) consisting of state-space layers that can be efficiently trained and configured for inference, 2) allowing for real-time inference with low latency, 3) architecturally simple and light in parameters and MACs, 4) capable of processing raw audio waveforms directly without requiring pre/post-processing, and 5) highly competitive with other speech enhancement solutions.

7. Acknowledgement

We thank Temi Mohandespour, Keith Johnson, and Nikunj Kotecha for contributing to the early stages of the project. We also thank M. Anthony Lewis, Douglas McLelland, Kristofor Carlson, and Chris Jones for providing useful feedback on the manuscript.

8. References

- [1] F. G. Germain, Q. Chen, and V. Koltun, "Speech denoising with deep feature losses," *arXiv preprint arXiv:1806.10522*, 2018.
- [2] J. Chen, J. Benesty, Y. Huang, and S. Doclo, "New insights into the noise reduction wiener filter," *IEEE Transactions on audio, speech, and language processing*, vol. 14, no. 4, pp. 1218–1234, 2006.
- [3] S. V. Vaseghi, *Advanced digital signal processing and noise reduction*. John Wiley & Sons, 2008.
- [4] V. Srinivasarao and U. Ghanekar, "Speech enhancement-an enhanced principal component analysis (epca) filter approach," *Computers & Electrical Engineering*, vol. 85, p. 106657, 2020.
- [5] C. Yu, R. E. Zecario, S.-S. Wang, J. Sherman, Y.-Y. Hsieh, X. Lu, H.-M. Wang, and Y. Tsao, "Speech enhancement based on denoising autoencoder with multi-branched encoders," *IEEE/ACM Transactions on Audio, Speech, and Language Processing*, vol. 28, pp. 2756–2769, 2020.
- [6] A. Azarang and N. Kehtarnavaz, "A review of multi-objective deep learning speech denoising methods," *Speech Communication*, vol. 122, pp. 1–10, 2020.
- [7] Z. Zhao, H. Liu, and T. Fingscheidt, "Convolutional neural networks to enhance coded speech," *IEEE/ACM Transactions on Audio, Speech, and Language Processing*, vol. 27, no. 4, pp. 663–678, 2018.
- [8] R. Giri, U. Isik, and A. Krishnaswamy, "Attention wave-u-net for speech enhancement," in *2019 IEEE Workshop on Applications of Signal Processing to Audio and Acoustics (WASPAA)*. IEEE, 2019, pp. 249–253.
- [9] A. Defossez, G. Synnaeve, and Y. Adi, "Real time speech enhancement in the waveform domain," *arXiv preprint arXiv:2006.12847*, 2020.
- [10] M. M. Kashyap, A. Tambwekar, K. Manohara, and S. Natarajan, "Speech denoising without clean training data: A noise2noise approach," *arXiv preprint arXiv:2104.03838*, 2021.
- [11] H.-S. Choi, J.-H. Kim, J. Huh, A. Kim, J.-W. Ha, and K. Lee, "Phase-aware speech enhancement with deep complex u-net," in *International Conference on Learning Representations*, 2018.
- [12] S. Pascual, A. Bonafonte, and J. Serra, "Segan: Speech enhancement generative adversarial network," *arXiv preprint arXiv:1703.09452*, 2017.
- [13] D. Rethage, J. Pons, and X. Serra, "A wavenet for speech denoising," in *2018 IEEE International Conference on Acoustics, Speech and Signal Processing (ICASSP)*. IEEE, 2018, pp. 5069–5073.
- [14] Y. Hu, Y. Liu, S. Lv, M. Xing, S. Zhang, Y. Fu, J. Wu, B. Zhang, and L. Xie, "Dccrn: Deep complex convolution recurrent network for phase-aware speech enhancement," *arXiv preprint arXiv:2008.00264*, 2020.
- [15] S. Zhao, B. Ma, K. N. Watcharasupat, and W.-S. Gan, "Frcrn: Boosting feature representation using frequency recurrence for monaural speech enhancement," in *ICASSP 2022-2022 IEEE International Conference on Acoustics, Speech and Signal Processing (ICASSP)*. IEEE, 2022, pp. 9281–9285.
- [16] C. Zheng, H. Zhang, W. Liu, X. Luo, A. Li, X. Li, and B. C. Moore, "Sixty years of frequency-domain monaural speech enhancement: From traditional to deep learning methods," *Trends in Hearing*, vol. 27, p. 23312165231209913, 2023.
- [17] J.-M. Valin, U. Isik, N. Phansalkar, R. Giri, K. Helwani, and A. Krishnaswamy, "A perceptually-motivated approach for low-complexity, real-time enhancement of fullband speech," *arXiv preprint arXiv:2008.04259*, 2020.
- [18] J.-M. Valin, "A hybrid dsp/deep learning approach to real-time full-band speech enhancement," in *2018 IEEE 20th international workshop on multimedia signal processing (MMSP)*. IEEE, 2018, pp. 1–5.
- [19] A. Defossez, G. Synnaeve, and Y. Adi, "Real time speech enhancement in the waveform domain," *arXiv preprint arXiv:2006.12847*, 2020.
- [20] Z. Kong, W. Ping, A. Dantrey, and B. Catanzaro, "Speech denoising in the waveform domain with self-attention," in *ICASSP 2022-2022 IEEE International Conference on Acoustics, Speech and Signal Processing (ICASSP)*. IEEE, 2022, pp. 7867–7871.
- [21] H. Schröter, T. Rosenkranz, A. Maier *et al.*, "Deepfilternet: Perceptually motivated real-time speech enhancement," *arXiv preprint arXiv:2305.08227*, 2023.
- [22] A. Gu, K. Goel, and C. Ré, "Efficiently modeling long sequences with structured state spaces," *arXiv preprint arXiv:2111.00396*, 2021.
- [23] K. Goel, A. Gu, C. Donahue, and C. Ré, "It's raw! audio generation with state-space models," in *International Conference on Machine Learning*. PMLR, 2022, pp. 7616–7633.
- [24] Z. Wang, X. Zhu, Z. Zhang, Y. Lv, N. Jiang, G. Zhao, and L. Xie, "Selm: Speech enhancement using discrete tokens and language models," in *ICASSP 2024-2024 IEEE International Conference on Acoustics, Speech and Signal Processing (ICASSP)*. IEEE, 2024, pp. 11 561–11 565.
- [25] A. Gu, K. Goel, A. Gupta, and C. Ré, "On the parameterization and initialization of diagonal state space models," *Advances in Neural Information Processing Systems*, vol. 35, pp. 35 971–35 983, 2022.

- [26] J. T. Smith, A. Warrington, and S. W. Linderman, "Simplified state space layers for sequence modeling," *arXiv preprint arXiv:2208.04933*, 2022.
- [27] Y. R. Pei and O. Coenen, "Building temporal kernels with orthogonal polynomials," *arXiv preprint arXiv:2405.12179*, 2024.
- [28] J. Gray and S. Kourtis, "Hyper-optimized tensor network contraction," *Quantum*, vol. 5, p. 410, 2021.
- [29] Y. Du, X. Liu, and Y. Chua, "Spiking structured state space model for monaural speech enhancement," in *ICASSP 2024-2024 IEEE International Conference on Acoustics, Speech and Signal Processing (ICASSP)*. IEEE, 2024, pp. 766–770.
- [30] P.-J. Ku, C.-H. H. Yang, S. M. Siniscalchi, and C.-H. Lee, "A multi-dimensional deep structured state space approach to speech enhancement using small-footprint models," *arXiv preprint arXiv:2306.00331*, 2023.
- [31] R. Chao, W.-H. Cheng, M. La Quatra, S. M. Siniscalchi, C.-H. H. Yang, S.-W. Fu, and Y. Tsao, "An investigation of incorporating mamba for speech enhancement," *arXiv preprint arXiv:2405.06573*, 2024.
- [32] X. Zhang, Q. Zhang, H. Liu, T. Xiao, X. Qian, B. Ahmed, E. Ambikairajah, H. Li, and J. Epps, "Mamba in speech: Towards an alternative to self-attention," *arXiv preprint arXiv:2405.12609*, 2024.
- [33] Y. R. Pei, S. Brüers, S. Crouzet, D. McLelland, and O. Coenen, "A Lightweight Spatiotemporal Network for Online Eye Tracking with Event Camera," in *Proceedings of the IEEE/CVF Conference on Computer Vision and Pattern Recognition Workshops*, 2024.
- [34] C. K. Reddy, V. Gopal, R. Cutler, E. Beyrami, R. Cheng, H. Dubey, S. Matussevych, R. Aichner, A. Aazami, S. Braun *et al.*, "The interspeech 2020 deep noise suppression challenge: Datasets, subjective testing framework, and challenge results," *arXiv preprint arXiv:2005.13981*, 2020.
- [35] R. Girshick, "Fast r-cnn," in *Proceedings of the IEEE international conference on computer vision*, 2015, pp. 1440–1448.
- [36] D. de Oliveira, S. Welker, J. Richter, and T. Gerkmann, "The pesqetarian: On the relevance of goodhart's law for speech enhancement," *arXiv preprint arXiv:2406.03460*, 2024.

A. Diagonalization of the \bar{A} matrix

If we allow \bar{B} and C to be complex matrices, then we can assume \bar{A} to be diagonal without any loss of generality. To see why, we simply let $\bar{A} = P^{-1}\Lambda_A P$ (where Λ_A is the diagonalized \bar{A} matrix, and P is the similarity matrix) and observe the following:

$$\begin{aligned} \forall t, \quad k[t] &= C(P^{-1}\Lambda_A P)^{t-1}\bar{B} \\ &= CP^{-1}\underbrace{\Lambda_A(PP^{-1})\dots\Lambda_A(PP^{-1})}_{\text{repeat } t-1 \text{ times}}P\bar{B} \\ &= (CP^{-1})\Lambda_A^{t-1}(P\bar{B}) \\ &= C'\Lambda_A^{t-1}\bar{B}', \end{aligned} \quad (7)$$

where \bar{B}' and C' are complex matrices that have “absorbed” the similarity matrix P , but WLOG we can just redefine them to be \bar{B} and C . Since \bar{A} is a real matrix, the complex eigenvalues in Λ_A must come in conjugate pairs. And WLOG we can again redefine Λ_A as \bar{A} .

B. Experiment Details

Our baseline model is trained using PyTorch with:

- 500 epochs
- AdamW optimizer with the PyTorch default configs
- A cosine decay scheduler with a linear warmup period equal to 0.01 of the total training steps, updating after every optimizer step
- gradient clip value of 1
- layer normalization (over the feature dimension) with elementwise affine parameters
- SiLU activation
- no dropout

The high-level training pipeline for the raw audio denoising model is to simply generate synthetic noisy audios by randomly mixing clean and noise audio sources. The noisy sample is then used as input to the model, and the clean sample is used as the target output.

For the clean training samples, we use the processed VCTK and LibriVox datasets that can be downloaded from the Microsoft DNS4 challenge. We also use the noise training samples from the DNS4 challenge as well, which contains the Audioset, Freesound, and DEMAND datasets. For all audio samples, we use the `librosa` library to resample them to 16 kHz and load them as numpy arrays.

For the LibriVox audio samples which form long continuous segments of human subjects reading from a book, we simply concatenate all the numpy arrays, and pad at the very end such that the array can be reshaped into (segments, 2^{17}). For all the other audio samples consisting of short disjoint segments, we perform intermediate paddings when necessary, to ensure a single recording does not span two rows in the final array. For audio samples longer than length 2^{17} , we simply discard them. The input length to our network during training is then also 2^{17} .

For every epoch, we use the entirety of the VCTK dataset and 10 percent of a randomly sampled subset of the LibriVox dataset. For each clean segment, we pair it with a randomly sampled noise segment (with replacement). The clean and noise samples are added together with an SNR sampled from -5 dB to 15 dB, and the synthesized noisy sample is then rescaled to a random level from -35 dB to -15 dB. Furthermore, we perform

random temporal and frequency masking (part of the SpecAugment transform) on only the input noisy samples.

For the loss function, we combine SmoothL1Loss with spectral loss on the ERB scale, without any equalization procedure on the raw waveforms or spectrograms. The β parameter of the SmoothL1Loss is set at 0.5, and the spectral loss is weighted by a factor that grows from 0 to 1 linearly during training. We use a learning rate of 0.005 and a weight decay of 0.02.

C. Network Details

C.1. Initialization of SSM Parameters

As mentioned in Section 2, we make the SSM parameters $\{A, B, C, \Delta\}$ trainable. Recall that we take $A \in \mathbb{C}^h$ to be a complex vector (or a complex diagonal matrix). For stability, we treat the real and complex parts of A separately. The real part $\Re(A)$ is parameterized as $-\text{softplus}(a_r)$, where a_r is initialized with the value -0.4328 , giving $\Re(A) = -1/2$ initially. Note that due to the positivity of softplus, $\Re(A)$ will always remain negative during training, which ensures the stability of the SSM layer. The imaginary part $\Im(a)$ is parameterized directly and initialized with $\pi(i-1)$ where i is the state index. The matrix $B \in \mathbb{R}^{h \times n}$ is initialized with all ones, and the matrix $C \in \mathbb{R}^{m \times h}$ is initialized with Kaiming normal random variables (assuming a fan in of h). Finally, we initialize Δ with $0.001 \times 100^{\lfloor i/16 \rfloor}$, giving a series of geometrically spaced values from 0.001 to 0.1 in blocks of 16. These initializations and parameterizations are not absolutely required, and we suspect that any reasonable approach respecting the stability of the SSM layer will suffice.

C.2. Optimal Contraction Order

If we let $K(t) = \bar{A}^t$ be the “basis kernels” of the SSM layer, and its Fourier transform be $\hat{K}(f)$, then in einsum form, the SSM layer operations during training can be expressed as

$$\hat{y}_{bjf} = \hat{x}_{bif}\bar{B}_{ni}\hat{K}_{nf}C_{jn} \quad (8)$$

by virtue of the convolution theorem, where $\{b, i, j, n, f\}$ indexes the batch size, input channels, output channels, internal states, and Fourier modes respectively. With abuse of notation, we similarly let $\{B, I, J, N, F\}$ be the sizes of the five aforementioned dimensions. Note that the number of Fourier modes F is the same as the length of the signal L (or roughly half of L for real FFT).

There are two main ways to compute \hat{y} . First, we can perform the operations of Eq. 8 from left to right normally, corresponding to projecting the input, performing the FFT convolution, then projecting the output. Alternatively, we can compute the full kernel, then perform the full FFT convolution with the input as $\hat{x}_{bif}(\bar{B}_{ni}\hat{K}_{nf}C_{jn})$. If we only focus on the computational requirements of the forward pass, then the first contraction order will result in $BNIF + BNF + BJNF \approx BNF(I + J)$ units of computation. The second contraction order will result in $JNI + JNIF + BJIF \approx JIF(B + N)$ units of computation. Therefore, we see that the optimal contraction order is intimately linked with the dimensions of the tensor operands. More formally, the first order of contraction is more optimal only when $BNF(I + J) < JIF(B + N)$ or $\frac{1}{B} + \frac{1}{N} > \frac{1}{I} + \frac{1}{J}$.

C.3. Network Latency

As mentioned in Section 3 and Fig. 1 of the main text, our model is an autoencoder network with long-range skip connections between the encoder and decoder blocks. Each SSM layer retains the length and channels of the input features, and a resampling layer performs both the temporal resampling and channel projection operations. For example, the first SSM block maps the input features as $(1, L) \rightarrow (1, L)$, followed by a resampling layer that maps the features as $(1, L) \rightarrow (16, L/4)$, through the process described in Section 3. The resampling factor and output channel of each block are reported in Table 1. For all blocks, the hidden state of the SSM layer is fixed to $h = 256$.

If the network does not have any (non-causal) convolutional layers (or PreConvs), then the theoretical latency can be simply determined from the product of the resampling factors, since the “stride sizes” is the same as the “kernel sizes” for these layers. In the case of the network given in Table 1, the product of the resampling factors (or the total resampling factor) is 256, and the sample rate of the input signal is 16000Hz, so the latency of the network is at least $256/16000\text{Hz} = 16$ milliseconds⁸. In the presence of PreConvs, or centered convolutional layers of kernel sizes of 3, there are additional latencies introduced due to the non-causal nature of the convolutions. More specifically, the additional latency is the look-forward timestep of the kernel, or simply the step size of the input features.

D. Importance of raw audio features

The aTENNuate network receives raw audios as inputs and produces raw audios as outputs directly, which gives rise to the natural hourglass macro-architecture where downsampling and upsampling operations are progressively performed. If we were to opt for a more traditional approach, the network would receive audio features that underwent STFT and produce audio features that will undergo iSTFT.

A typical window size and hop length for these spectral transform operations are 512 samples (32 ms) and 256 samples (16 ms), respectively. This would effectively yield 257 complex features as input to the network (up to the Nyquist frequency). If we omit the DC component (which can be “absorbed” into the biases of the network), then we are effectively left with 256 complex channels. Naturally, we can then build a homogeneous variant of the aTENNuate network by simply stacking the bottleneck blocks, which also expect channels of 256. Here, we choose to repeat the block 12 times, with nested skip connections as prescribed in the original network.

In Table 5, we see that despite requiring more parameters and MACs, the homogeneous network working with spectral features did not outperform the aTENNuate network working with raw audios.

Table 5: Comparing the aTENNuate raw-audio denoising network against a 12-layer homogeneous S5 network working with spectral features. Both networks contain no PreConv layers, and has a network latency of 16 ms. Note the computational costs of STFT and iSTFT operations are not accounted for.

Model	PESQ	Parameters	MACs / sec
aTENNuate	3.06	0.84M	0.33G
aTENNuate (STFT + iSTFT)	2.72	1.58M	1.59G

⁸Technically, it should be $(256 - 1)/16000\text{Hz} = 15.9\text{ms}$, but this makes little difference.